Title
PROCESSING PARAMETERS AND THE PROPERTIES OF LITHIUM FERRITE SPINEL

Authors
Bandyopadhyay, G.
Fulrath, R.M.

Publication Date
1973-07-01

Submitted to Journal of Am. Ceramic Society

LBL-1875
Preprint

PROCESSING PARAMETERS AND THE PROPERTIES OF LITHIUM FERRITE SPINEL

G. Bandyopadhyay and R. M. Fulrath

July 1973

Prepared for the U. S. Atomic Energy Commission
under Contract W-7405-ENG-48

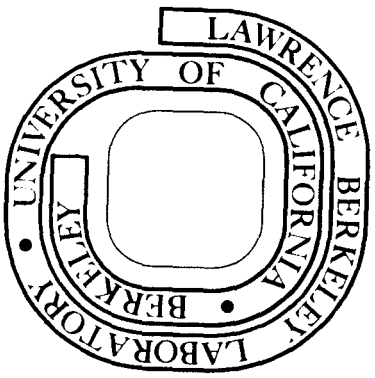

LBL-1875

DISCLAIMER

PROCESSING PARAMETERS AND THE PROPERTIES OF LITHIUM FERRITE SPINEL

G. Bandyopadhyay and R. M. Fulrath

Inorganic Materials Research Division, Lawrence Berkeley Laboratory
and Department of Materials Science and Engineering,
College of Engineering; University of California,
Berkeley, California 94720

ABSTRACT

Polycrystalline compacts of lithium ferrite with varying stoichiometry were sintered using a packing powder technique and high oxygen atmosphere to control the material loss from the system. These specimens were used to study the influence of sintering time and temperature, and stoichiometry on the densification, microstructural chracteristics, dc resistivity, and hysteresis loop parameters of lithium ferrite. The influence of the packing powder composition was also investigated.

I. INTRODUCTION

Lithium ferrite spinel ($LiFe_5O_8$) has attracted considerable attention[1-4] because of its square loop properties coupled with the superior temperature stability. It is well known that during sintering, lithium ferrite tends to lose oxygen and lithium. Until very recently,[1-2] little attention was given to characterize the material loss behavior and its effect on the properties of the final sintered ceramic. Most of the previous work controlled the oxygen atmosphere during the sintering process to control the oxygen loss from the system. No attempts were made to control lithium loss. In this investigation, a packing powder technique, as has been used extensively for the processing of lead zirconate titanate ceramic,[5] has been employed to control lithium loss from the system. In the process, various sintering parameters and stoichiometry have been correlated with the densification, microstructural characteristics, dc resistivity, and hysteresis loop parameters of lithium ferrite.

II. EXPERIMENTAL PROCEDURE

(1) Powder and Specimen Preparation

Reagent grade Li_2CO_3 and Fe_2O_3 were mixed in suitable proportion in a neoprene lined ball mill for 48 h using isopropyl alcohol and teflon balls as the mixing media. The alcohol was evaporated off and the mixture was calcined at 800°C for 6 h. The powder was milled again and kept ready for sample preparation. X-ray diffraction of this powder detected traces of $LiFeO_2$ and α-Fe_2O_3 in the composition. But from now on, this powder will be termed as "stoichiometric powder."

$LiFeO_2$ powders were also prepared in the identical way using suitable proportions of Li_2CO_3 and Fe_2O_3.

In order to make a series of powders with known deviations from the stoichiometric composition, $LiFe_5O_8$ was mixed with proper proportions of $LiFeO_2$ or Fe_2O_3 in a ball mill as described above for 24 h. The packing powders were prepared in the same way except that the last milling was eliminated to keep the particle size somewhat coarse.

Specimens, 1 in. diameter and 1/4 in. thick, were prepared by cold pressing. Sample weight and size were controlled to control the green density of all the specimens to approximately 53% of the theoretical value.

(2) Sintering Conditions

Isothermal sintering runs at 1 atm O_2 and using a stoichiometric packing powder were carried out at four different temperatures (1100°, 1150°, 1200°, 1250°C). Specimens were always burried deep into the packing powder and, to keep the uncertainties to a minimum, the same amount of packing powder was used in all the sintering runs.

In order to study the influence of nonstoichiometry on various properties, standard specimens of different starting compositions were sintered at 1150°C for 2 h in 1 atm O_2 and using stoichiometric packing powder. In some cases stoichiometric specimens were used and the packing powder composition was varied.

(3) Property Measurement

Density of the sintered specimens were measured by water displacement and also by geometric measurements. Theoretical density for the stoichiometric lithium ferrite composition was taken as 4.752 gs/cc.

Corrections were made for any change in the starting composition.

For the microstructural investigation, specimens were polished and then thermally etched at 975°C for 15 min as suggested by West and Blankenship.[6] For some compositions, a longer time was necessary.

DC resistivity was measured by using a guard ring method (Fig. 1). Indium amalgam was used as the electrode material and standard sized specimens were used. Extremely reproducible data were obtained by using this method and it was possible to simultaneously measure the bulk and surface resistivity of a specimen.

Hysteresis loop parameters were measured from a B-H curve taken at 60 Hz obtained by using a torroidal shape specimen. The size of the specimens for these measurements was 0.8 in. O.D., 0.5 in. I.D. and 1/4 in. thick. Sixty turns of copper magnet wire were used in both primary and secondary windings.

III. RESULTS AND DISCUSSION

(1) Isothermal Sintering

Coble[7] has derived the following relation for bulk diffusion sintering applicable to later stages

$$d\rho/dt = ND\gamma\Omega/l^3kT \qquad (1)$$

where $d\rho/dt$ is the densification rate, N is a numerical constant, D is the diffusion coefficient, γ is the surface energy, Ω is a vacancy volume, l is the grain size and kT has the usual significance. If we assume that at a particular density, where discontinuous grain growth has not started, the average grain size is always equal irrespective of

the temperature at which the sintering has been carried out, Eq. (1) can be integrated. Then, on rearrangement and substituting $D = D_o \exp(-Q/kT)$ one can get

$$T/t = (N\gamma\Omega D_o/(\rho-C)kl^3)\cdot\exp(-Q/kT) \qquad (2)$$

where C is an integration constant. Thus we should be able to determine the activation energy for the rate controlling diffusional process from the slope of log(T/t) vs 1/T plot. This plot is shown in Fig. 2 for a density of 95% of theoretical value. The activation energy is found to be 143 kcal/mol. The assumption of constant grain size, which has been made above, was found to be reasonable. The microstructural studies revealed an average grain size of 3-5 microns in all the specimens at 95% TD.

(2) Nonstoichiometry and Its Relation to Densification and Microstructure

The effect of nonstoichiometry on the sinter density and microstructure of ferrites was first reported by Stuijts.[8,9] Reinjnen[10-12] afterwards presented an adequate theoretical model along with the experimental support, based on the assumption of volume diffusion, to describe the influence of stoichiometry on the sintering of spinels, oxides and oxidic compounds. Readey[13] also calculated the dependence of volume diffusion on small deviations from stoichiometry. In Reinjnen's analysis it was assumed that, in the spinels diffusivity of oxygen, (D_{oxygen}) is much smaller than the diffusivity of cations (D_c). Under this condition, it was shown that the vacancy flux reduces drastically in the region of

excess cation vacancies. Accordingly, he showed in the case of $NiAl_2O_4$ system, a drastic drop in the sinter density in the excess Al_2O_3 compositions which is the cation deficient side of the system. But the density drop was much less drastic in the $NiFe_2O_4$ system under the same conditions. This was accounted for on the basis that Fe_2O_3 is mainly dissolved as Fe_3O_4 and partly as Fe_2O_3. Sintering at high temperatures results in further reduction of Fe^{+3} to Fe^{+2} by the reaction

$$Fe^{+3} + 3/8V_c + 1/2\ O^{-2} \rightleftarrows Fe^{+2} + 1/4\ O_2(g) \qquad (3)$$

and thus a large part of the excess cation vacancies are annihilated resulting in an increase of anion vacancy concentration. Stuijts[14] later on reviewed Reinjnen's results and showed strikingly similar behavior in the densification of Ni-Zn ferrite composition with the theoretical plot of Reinjnen.

Similar studies on the lithium ferrite system has been done in this investigation. Figure 3 shows the relationship between the sinter density and the composition of the green compact (solid line). As is expected, maximum density was obtained slightly on the lithia rich side. It is also clear that the density drops significantly in the Fe_2O_3 excess region.

The microstructural characteristics observed on these sintered specimens are also in agreement with Stuijts'[8,9] or Reinjnen's[10] observation for other ferrites. As shown in Fig. 4, compositions with excess Fe_2O_3 showed a microstructure with large pores exclusively at the grain corners. On the other hand, the lithia rich compositions showed

discontinuous grain growth with pores entrapped within the grains.

In all the above runs, stoichiometric packing powder and 1 atm O_2 were used for atmosphere control. For the varying composition packing powders, stoichiometric specimens were used. In Fig. 3, density values have been plotted against the composition of the packing powder (dashed line). It is expected that with a Fe_2O_3 rich packing powder some lithia will be lost from the specimen, thus leading to an excess Fe_2O_3 in the specimen composition. On the other hand, the lithia content may be kept constant in the specimen with the lithia rich packing powder. Since the excess Fe_2O_3 in the former composition would mean a higher cation vacancy concentration (and hence a lower anion vacancy concentration), a lower density is expected when Fe_2O_3 rich packing powders are used in the sintering runs. The insignificant density difference as observed at 1150°C (Fig. 3) may be due to the loss of excess cation vacancies through the oxygen loss by reaction 3. Thus if the oxygen loss could be avoided by using a lower sintering temperature so that the cation vacancies would remain low, a significant density difference should be observed depending on the packing powder composition. This has been found to be true as shown in Fig. 5 where Lacy's[15] data has been plotted. It is clear that sintering at 1000°C results in a density difference of about 10%, whereas at 1100°C almost the same densities are attained under both conditions.

(3) X-ray Results

In the system Li_2O-FeO-Fe_2O_3 it is quite difficult to distinguish one phase from another by X-ray diffraction, because the important X-ray peaks for most of the possible phases (e.g. $LiFe_5O_8$, $LiFeO_2$, Fe_3O_4, etc)

overlap on one another. But by the use of I_{311}/I_{400} ratio (both the planes are for the spinel phases Fe_3O_4 and $LiFe_5O_8$; the (200) peak of $LiFeO_2$ overlaps with the (400) peak of the spinel phases), qualitative information about the relative amounts of spinel phase and $LiFeO_2$ phase can be obtained. A high value of the ratio indicates the predominance of the spinel phases whereas a low value would mean a large amount of $LiFeO_2$ in the composition. In Fig. 6, I_{311}/I_{400} ratio for the surface compositions of the sintered ferrites has been plotted against the composition of the green compact. Predominantly spinel phase was observed on the Fe_2O_3 rich side of the composition and $LiFeO_2$ phase on the lithia rich side. The bulk of all these specimens were X-rayed after grinding off the surface. In each case it showed X-ray peaks typical of the spinel. The composition variation at the surface of the sintered specimens is obviously due to the material loss from the system. Salmon and Marcus[16] first postulated the following reactions while studying the lithium loss behavior from a Li-Ni ferrite composition

$$6LiFe_5O_8(s) \rightleftarrows 6LiFeO_2(s) + 8Fe_3O_4(s) + 2O_2(g) \qquad (4)$$

$$6LiFeO_2(s) \rightleftarrows 2Fe_3O_4(s) + 3Li_2O(g) + 1/2\ O_2(g) \qquad (5)$$

Thus, according to these reactions, with the initial oxygen loss from the stoichiometric composition, $LiFeO_2$ phase should start to appear. Now if the conditions are such that the lithia loss is not possible by reaction 5, Fe_3O_4 may start to go into solid solution with $LiFeO_2$ as

FeO and thus a surface composition with no or very little spinel phase may be obtained. Apparently this is what happens with lithia excess composition. For Fe_2O_3 excess compositions, it appears as if Fe_2O_3 goes into solid solution with spinel $LiFe_5O_8$ as Fe_3O_4, and then the process stops unless the sintering temperature is high enough or the time at temperature is long enough to support further oxygen loss or lithia loss from the system. In Fig. 7, I_{311}/I_{400} ratio has again been plotted against sintering time at various temperatures. The green specimens in these runs were stoichiometric. The initial drop of the intensity ratio is probably due to the start of the reaction 4 when $LiFeO_2$ is formed. At higher temperature sintering runs (e.g. at 1150°, 1250°C), the ratio starts to increase again indicating the increase in the spinel content of the composition. This is probably because the lithia loss through reaction 5 gradually becomes significant at this point.

Predominantly spinel phase in the bulk composition is attributed to the very little material loss from the bulk region due to the formation of protective reacted layers.

(4) DC Resistivity

The influence of composition on the dc resistivity value of sintered polycrystalline lithium ferrite has been shown in Fig. 8. Both the bulk and the surface resistivity values are plotted. The sharp drop in the resistivity value while moving into the cation deficient region is similar to that observed for Ni-Zn ferrite[17] or for cobalt ferrite.[18] In the cases of Ni-Zn ferrite or cobalt ferrite, it has been shown that hole conduction due to Ni^{+3} or Co^{+3} dominates on the anion deficient side and electron conduction (due to Fe^{+2}) dominates in the cation deficient

region. The situation is somewhat different in the case of lithium ferrite where, unlike nickel or cobalt, lithium is monovalent and does not change valency. Another important point of difference is the tendency to order[19] in the octahedral region, which also has a strong influence on the conductivity value.[6,20,21] In any event, electron hopping from Fe^{+2} to Fe^{+3} has been found[21-23] to be the primary charge transfer mechanism in the conduction process of lithium ferrite. Wang et al.[21,22] in their investigation described oxygen vacancies as the minor carriers. For dc conductivity and for one type of charge carrier

$$\sigma = ne\mu \tag{6}$$

where n is the number of carriers and can be related to the number of Fe^{+2} ions in the octahedral site, e is the electronic charge and μ is the mobility of the electrons in the system. Jonker[18] expressed carrier mobility in cobalt ferrite by a diffusion type expression

$$\mu = (ed^2\nu/kT)\cdot\exp(-q/kT) \tag{7}$$

where d is the jump length, ν is the lattice frequency active in the jumping process and q is the activation energy for the jump. With increasing Fe_2O_3 in the composition, more and more Fe^{+2} would be active in charge transport. But at the same time Fe^{+2} in the octahedral region would tend to introduce some disorder in the system. As suggested by Austin and Mott[24] this disorder may contribute to the activation energy term (q) in the mobility expression (Eq. (7)), and thus decrease the

mobility of the carrier. The sharp drop in resistivity in the cation deficient region as shown in Fig. 8 is probably due to the increase in the number of charge carriers. But the changes that are observed away from the stoichiometric line can be due to a combined effect of mobility and charge carriers. In the anion deficient side, oxygen vacancies may act as the major carriers. But it is accepted[25] that too great a deviation from stoichiometry in the oxygen deficient region is unfavorable in lithium ferrite. Thus second phases show up rather quickly as has been confirmed by the microstructural investigation, and thus the resistivity of the system tends to increase.

Until now we have considered the resistivity problem only from the standpoint of carrier concentration and mobility term. For a polycrystalline sintered specimen, the problem may increase manyfold. In Fig. 9 average size of the largest grains and dc resistivity have been plotted against sintering time in isothermal sintering runs. It is clear that discontinuous grain growth is always accompanied by an increase of resistivity value. This is possible only if grain boundaries act as the easy conducting path compared to the bulk of the grains. This may be due to higher carrier concentration at the boundaries because of preferential material loss from or along the grain boundaries.

(5) B-H Loop Parameters

It has been reported in the literature[6,26-29] that with proper processing and with selected dopants very good square loop materials can be obtained from lithium ferrite compositions. The use of packing powder method for the processing of lithium ferrite also gave very good square loops. In most of the cases the squareness R_s, which has been

defined as the ratio of the remanent induction to the maximum induction (B_{max}), was found to be better than 0.85.

The influence of composition on the coercive force (H_c) has been shown in Fig. 10 (solid line). Decrease of H_c on the anion deficient region is probably due to the increased grain size. Compositional effect on the squareness or B_{max} value was found to be insignificant. The influence of the packing powder composition on the H_c value of the specimens sintered from the stoichiometric green compacts has also been shown in Fig. 10 (dotted line). Lower values of H_c were obtained by the use of lithia rich packing powder. One specimen was sintered in 1 atm O_2 without any packing powder. H_c value for this specimen has been represented by the star (*) in Fig. 10.

The effect of sintering time and temperature on the hysteresis loop parameters has been shown in Fig. 11. H_c drops to a low value with increasing time and temperature, B_{max} reaches a more or less constant value after long time sintering at any temperature. But squareness (R_s) showed a maxima with sintering time. These variations are probably a combined effect of density and microstructure evolution. With increasing density all the hysteresis loop parameters improve. But the strongest influence of the microstructural characteristics is probably on the H_c value, and thus in most of the above cases we see a drastic variation of the coercive force with the processing parameters.

IV. SUMMARY

The important conclusions are:

(1) The activation energy for the sintering of lithium ferrite was found to be 143 kcal/mol.

(2) Stoichiometry of the starting composition had a pronounced effect on most of the properties that were investigated. Anion deficient compositions led to denser specimens with higher dc resistivity values and squarer B-H loops having low coercive forces. But discontinuous grain growth was favored in these compositions.

(3) Dc resistivity of polycrystalline specimens were strongly dependent on the microstrucutre. It is postulated that the grain boundaries acted as the higher conducting path in these systems.

(4) The packing powder composition also significantly affected the properties of the sintered ceramic. The strongest influence was observed on the coercive force.

ACKNOWLEDGMENT

This work was supported by the U. S. Atomic Energy Commission through the Inorganic Materials Research Division of the Lawrence Berkeley Laboratory.

REFERENCES

1. A. J. Pointon and R. C. Saull, "Solid State Reactions in Lithium Ferrite," J. Am. Ceram. Soc., 52 [3] 157-160 (1969).

2. D. H. Ridgley, H. Lessof and J. D. Childress, "Effects of Lithium and Oxygen Losses on Magnetic and Crystallographic Properties of Spinel Lithium Ferrite," J. Am. Ceram. Soc., 53 [6] 304-311 (1970).

3. Yu. D. Tretyakov, N. N. Oleynikov, Yu. G. Metlin and A. P. Erastova, "Phase Equilibria and the Thermodynamics of Coexisting Phases in the System Iron-Lithium-Oxygen," J. Solid State Chem., 5 191-199 (1972).

4. Other references are compiled in ref. 2.

5. R. B. Atkin, Ph.D. thesis at the University of California, Berkeley, 1970.

6. R. G. West and A. C. Blankenship, "Magnetic Properties of Dense Lithium Ferrites," J. Am. Ceram. Soc., 50 [7] 343-349 (1967).

7. R. L. Coble, "Sintering Crystalline Solids: 1. Intermediate and Final State Diffusion Models," J. Appl. Phys., 32 [5] 787-792 (1961); "II. Experimental Test of Diffusion Models in Powder Compacts," ibid, pp. 793-799.

8. A. L. Stuijts, "Low Porosity Ferrites," Proc. Brit. Ceram. Soc., 2 73-81 (1964).

9. A. L. Stuijts, "Microstructural Considerations in Ferromagnetic Ceramics," Ceramic Microstructure, R. M. Fulrath and J. A. Pask, eds., (John Wiley and Sons, New York, 1968), pp. 443-474.

10. P. Reinjnen, "Sintering Behavior and Microstructures of Aluminates and Ferrites with Spinel Structure," Science of Ceramics, 4, 169-188 (1968).

11. P. Reinjnen, "Non-Stoichiometry and Sintering of Ionic Solids," Reactivity of Solids, J. W. Mitchell, R. C. Devries, R. W. Roberts and P. Cannon, eds., (John Wiley and Sons, New York, 1969), pp. 99-114.

12. P. Reinjnin, "Non-Stoichiometry and Sintering in Ionic Solids," Problems of Nonstoichiometry, A. Rabenau ed., (North Holland Publishing Co., Amsterdam, 1970), pp. 219-238.

13. D. W. Readey, "Mass Transport and Sintering in Impure Ionic Solids," J. Am. Ceram. Soc., 49 [7] 366-369 (1966).

14. A. L. Stuijts, "Control of Microstructures in Ferrites, 'Ferrites: Proceedings of the International Conference,' Y. Hoshino, S. Iida and M. Sugimoto eds., (University of Tokyo Press, 1971), pp. 108-113.

15. A. M. Lacy, unpublished work at the University of California, Berkeley, 1970.

16. O. N. Salmon and L. Marcus, "Note on Sublimation of Lithium from Li-Ni Ferrite," J. Am. Ceram. Soc., 43 [10] 549-550 (1960).

17. L. G. Van Uitert, "Dc Resistivity in the Nickel and Nickel Zinc Ferrite System," J. Chem. Phys., 23 [10] 1883-1887 (1955).

18. G. H. Jonker, "Analysis of the Semiconducting Properties of Cobalt Ferrite," J. Phys. Chem. Solids, 9 165-175 (1959).

19. P. B. Braun, "Superstructure in Spinels," Nature (London), 170 1123-1124 (1952).

20. E. Kato, "Phase Transition of Li_2O-Fe_2O_3 System II. Thermal and Electric Properties of Lithium Ferrospinel $LiFe_5O_8$," Bull. Chem. Soc. Japan, 31 [1] 113-117 (1958).

21. F. F. Y. Wang, R. L. Gravel and M. Kestigian, "Effect of Heat Treatment on the Electrical Resistivity of Lithium Ferrite," IEEE Trans. on Mag., MAG-4 [1] 55-58 (1968).

22. F.F.Y.Wang, R. L. Gravel and M. Kestigian, "Hall Effect in Single Crystal Lithium Ferrite," J. Appl. Phys., 38 [3] 1131-1132 (1967).

23. D. Elwell and D. S. Tanhauser, "The Hall Effect in Lithium Ferrite," Solid State Comm., 8 179-181 (1970).

24. I. G. Austin and N. F. Mott, "Polarons in Crystalline and Non-Crystalline Materials," Adv. Phys., 18 41-102 (1969).

25. D. W. Strickler and R. Roy, "Studies in the System Li_2O-Al_2O_3-Fe_2O_3-H_2O," J. Am. Ceram. Soc., 44 [5] 225-230 (1961).

26. H. P. J. Wijn, W. R. Gorter, C. J. Esveldt and P. Geldermans, "Conditions for Square Hysteresis Loops in Ferrites," Philips Tech. Rev., 16 [2] 49-58 (1954).

27. R. G. West, "Square Loop Properties of Lithium-Nickel-Zinc Ferrites," J. Appl. Phys., 34 [4, Pt 2] 1113-1114 (1963).

28. E. A. Schwabe and D. A. Campbell, "Influence of Grain Size on Square-Loop Properties of Lithium Ferrites," J. Appl. Phys., 34 (4, Pt 2] 1251-1253 (1963).

29. D. B. Rogers, R. W. Germann and R. J. Arnott, "Effect of Trivalent Manganese on the Crystal Chemistry of Some Lithium Spinels," J. Appl. Phys., 36 [8] 2338-42 (1965).

FIGURE CAPTIONS

Figure 1 - Guard ring set up for dc resistivity measurement.

Figure 2 - Log (T/t) vs 1/T relationship for specimens with 95% theoretical density. Sintering runs were done in 1 atm oxygen and with stoichiometric packing powder. Activation energy for the sintering, determined from the slope, is 143 kcal/mol.

Figure 3 - Variation of the sinter density with the composition of the specimen, and also with the composition of the packing powder. Sintering conditions were 1150°C for 2 h in 1 atm oxygen.

Figure 4 - Dependence of the microstructure on the stoichiometry. (A) $LiFe_5O_8$ + 1 mol% Fe_2O_3, (B) $LiFe_5O_8$ + 1 mol% $LiFeO_2$. Sintering runs were done at 1150°C for 2 h in 1 atm O_2 and using stoichiometric packing powder.

Figure 5 - Density-time relationship for some isothermal sintering runs of stoichiometric specimens in two different packing powder atmosphere and at 1 atm oxygen.[15]

Figure 6 - X-ray data for specimens sintered at 1150°C for 2 h in 1 atm oxygen using stoichiometric packing powder.

Figure 7 - X-ray data for isothermally sintered specimens. Sintering runs were done in 1 atm oxygen and with stoichiometric packing powder.

Figure 8 - Dependence of bulk and surface resistivity on the stoichiometry of the specimen. Sintering conditions were: temperature = 1150°C, time = 2 h, atmosphere = 1 atm oxygen and stoichiometric packing powder.

Figure 9 - Grain size and bulk resistivity data from some isothermal sintering runs. Stoichiometric packing powder and 1 atm oxygen were used in all the sintering runs.

Figure 10 - Variation of coercive force (H_c) with the composition of the specimen, and also with the composition of the packing powder. Specimens were sintered at 1150°C for 2 h in 1 atm oxygen.

Figure 11 - Variation of B-H loop parameters with sintering time in some isothermal sintering runs. Stoichiometric packing powder and 1 atm oxygen were used in all these runs.

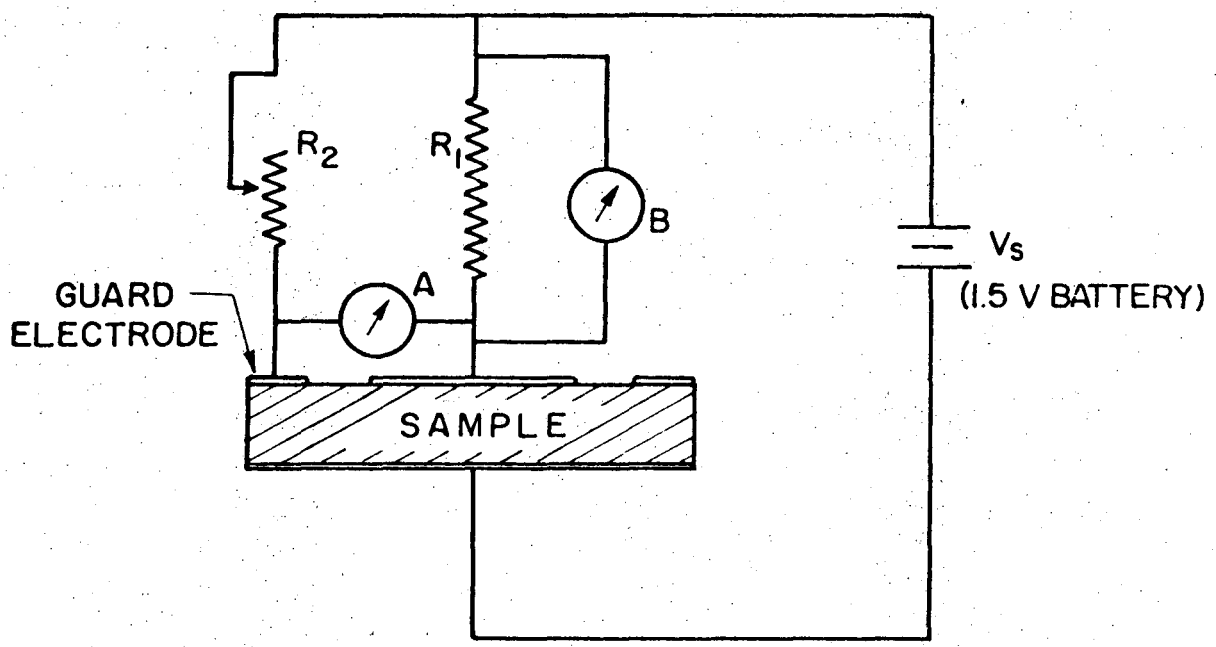

R_1 CONSTANT RESISTANCE

R_2 VARIABLE RESISTANCE

A NULL INDICATOR

B KEITHLEY ELECTROMETER

XBL 737-1578

Fig. 1

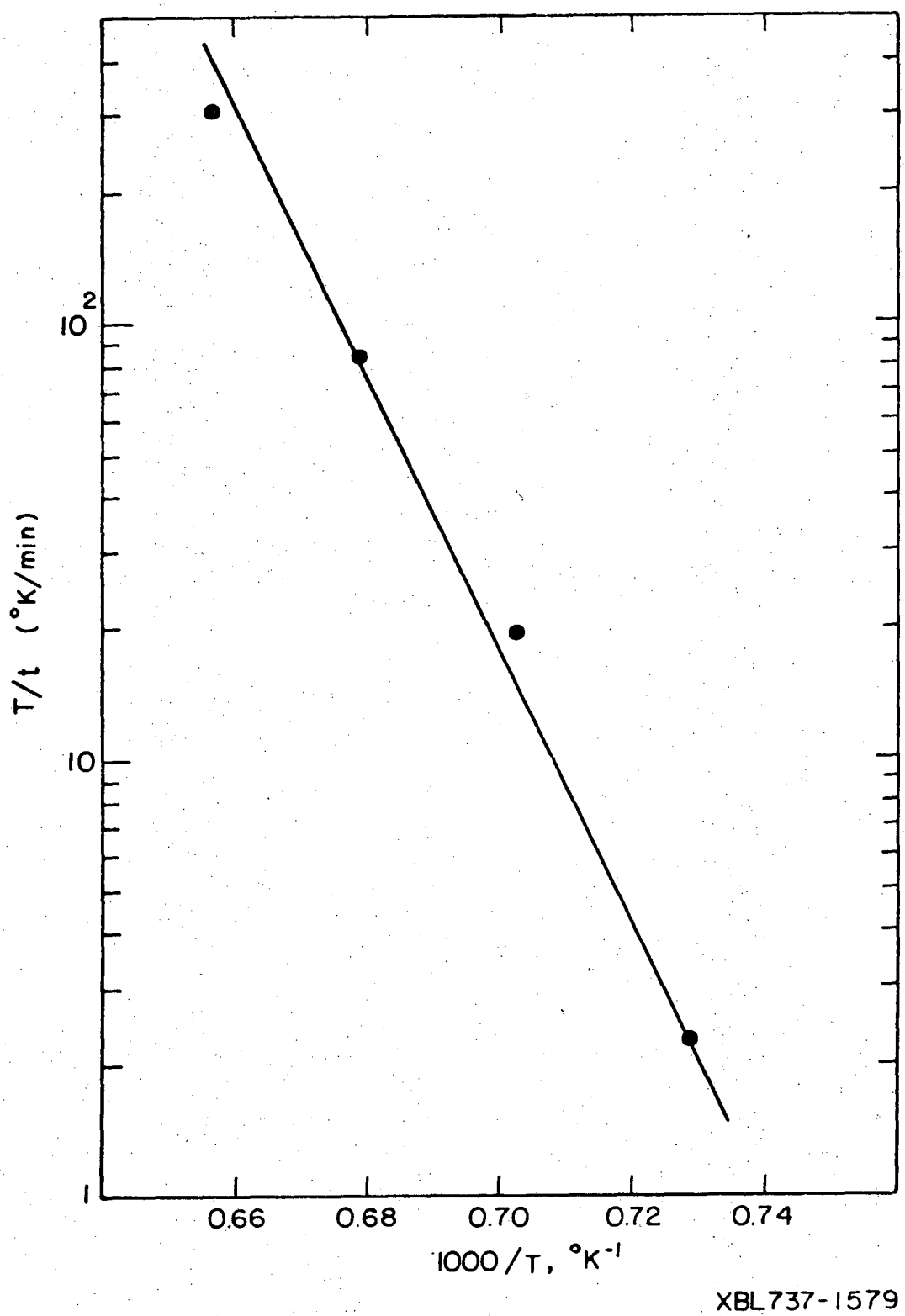

Fig. 2

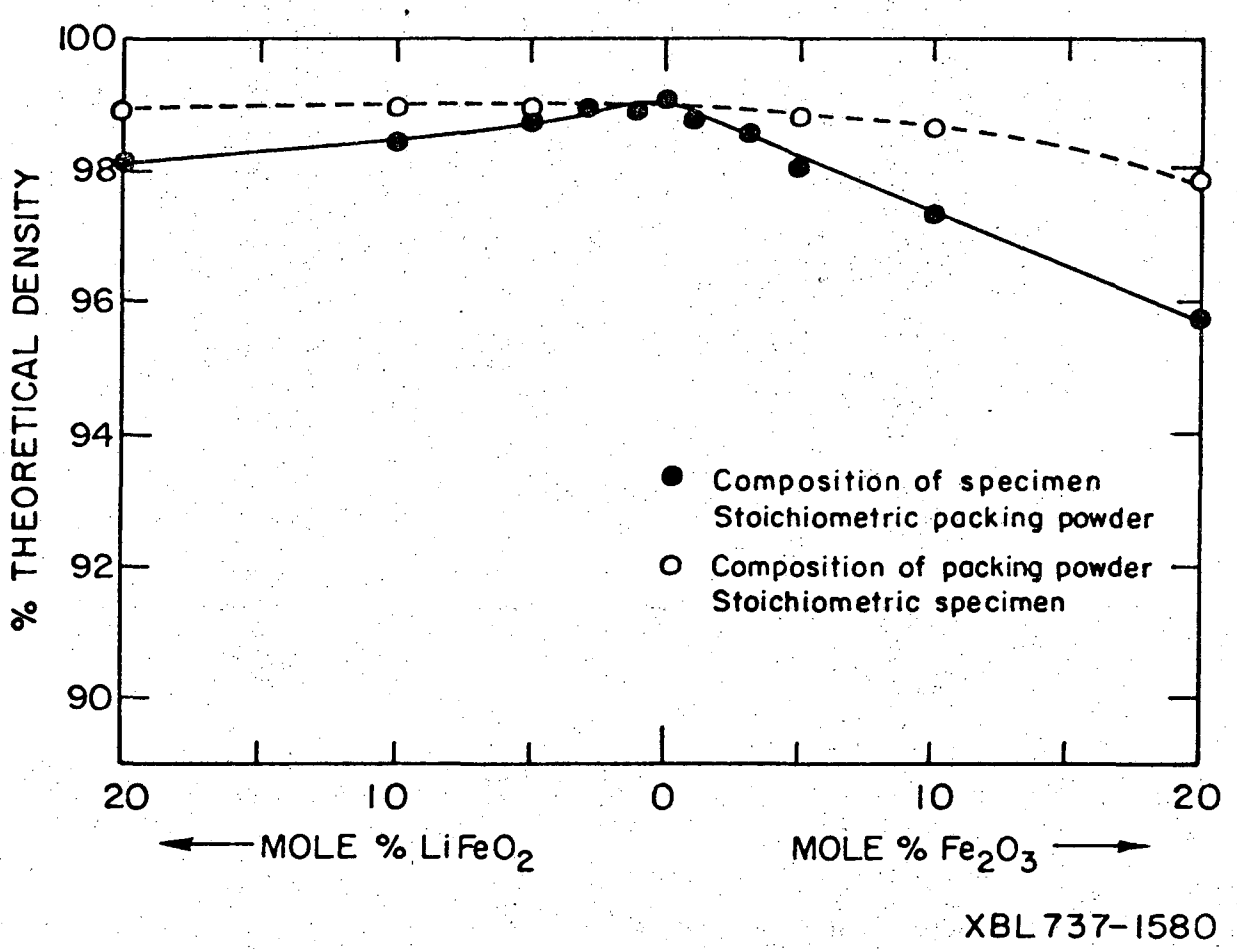
100
98
96
94
92
90
% THEORETICAL DENSITY
Composition of specimen
Stoichiometric packing powder
Composition of packing powder
Stoichiometric specimen
20
10
0
10
20
← MOLE % LiFeO2
MOLE % Fe2O3 →
XBL737-1580

Fig. 3

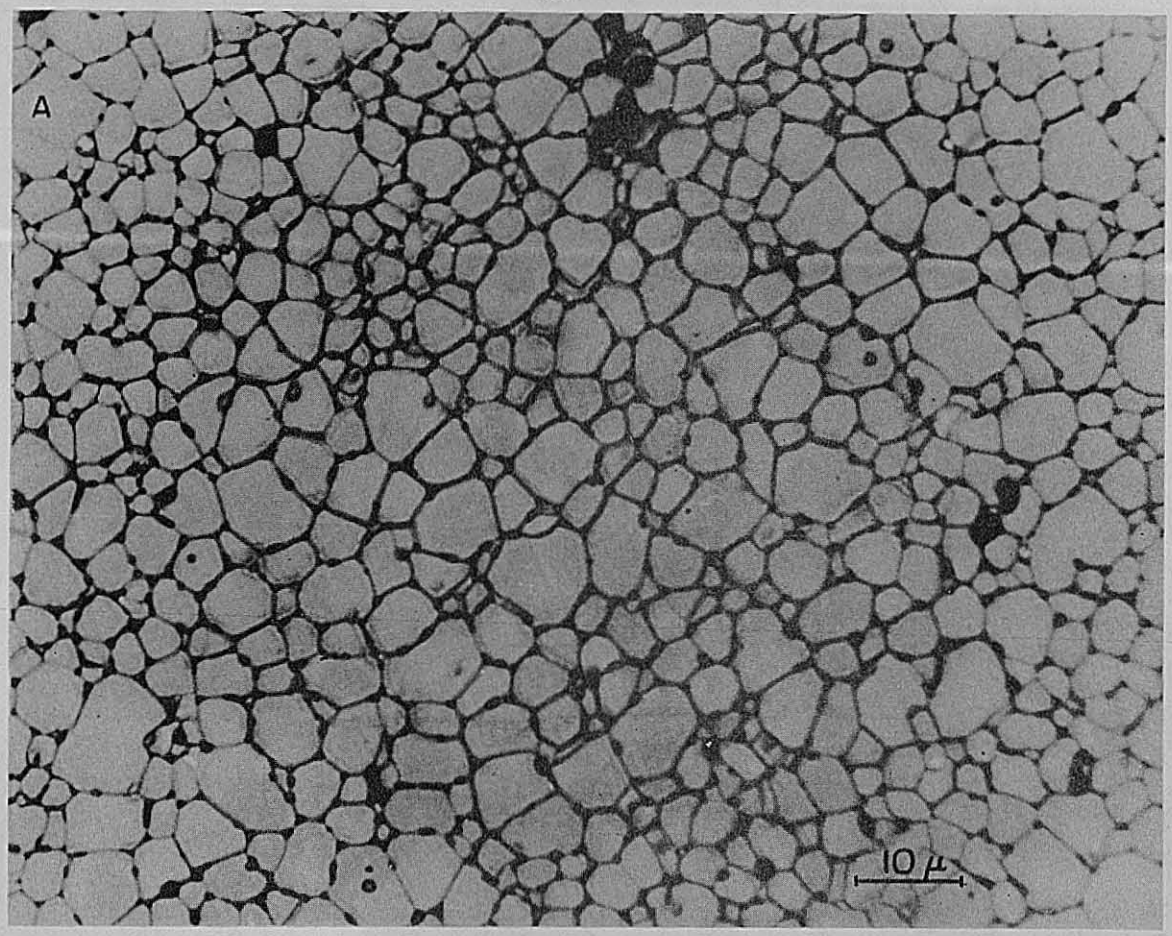

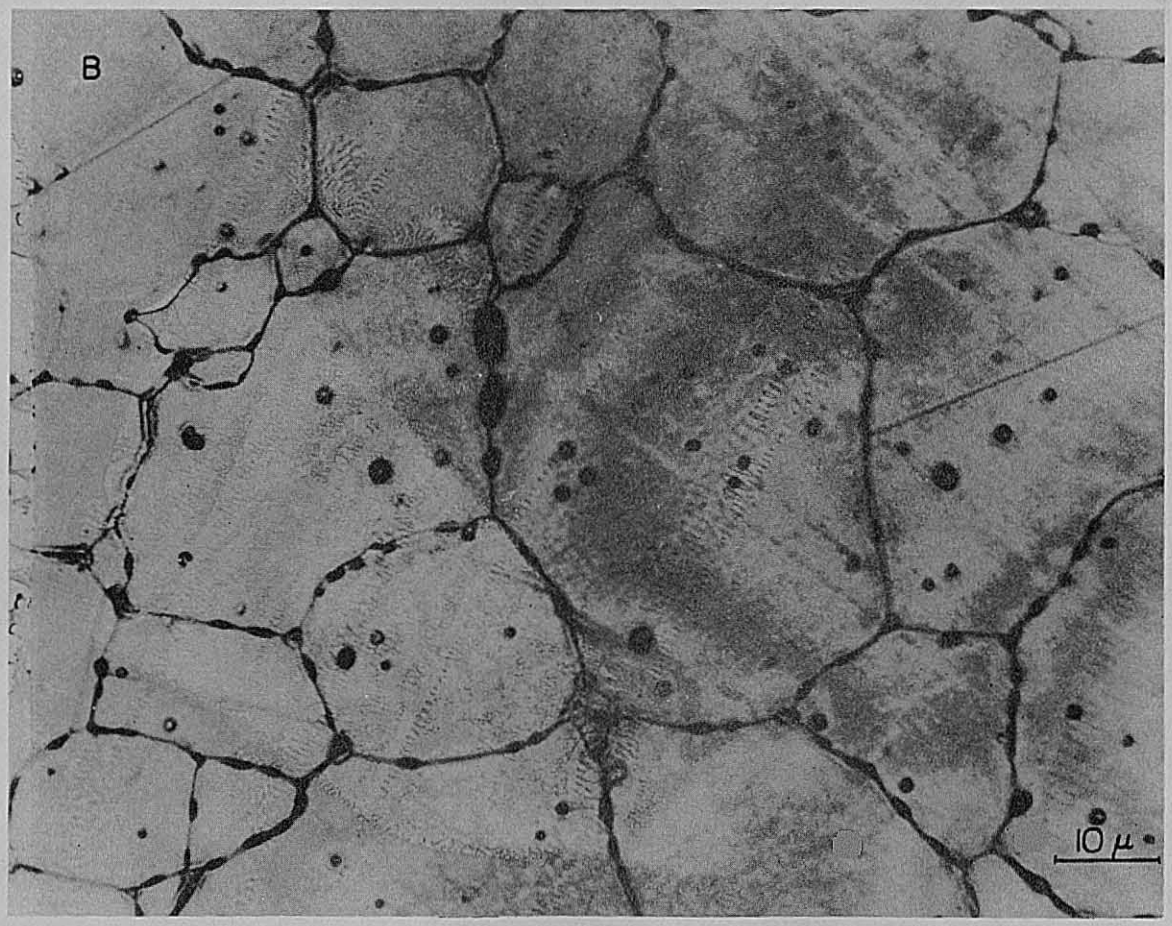

Fig. 4

XBB 737-4457

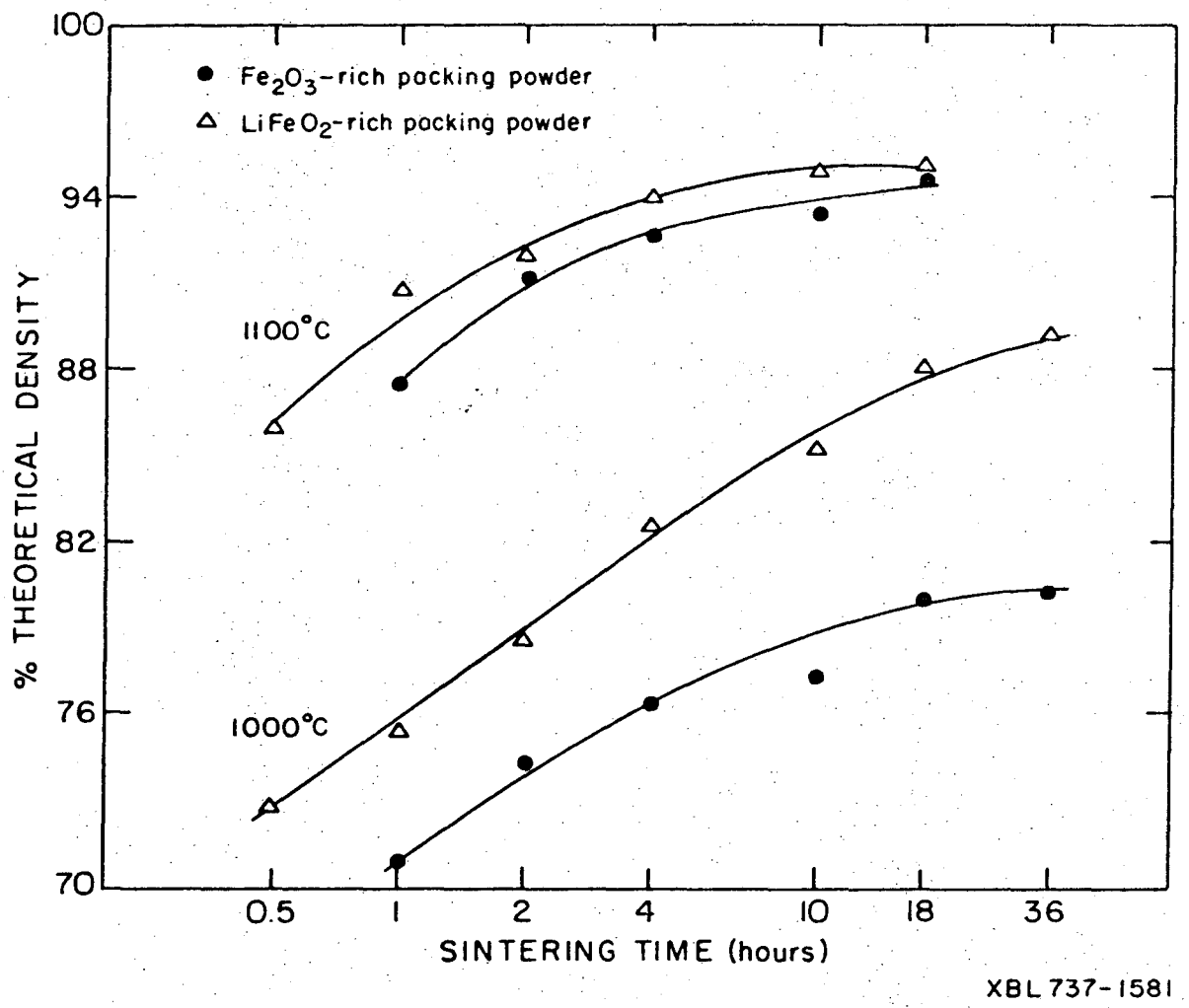
100
94
88
82
76
70
% THEORETICAL DENSITY
● Fe_2O_3-rich packing powder
△ $LiFeO_2$-rich packing powder
1100°C
1000°C
0.5
1
2
4
10
18
36
SINTERING TIME (hours)
XBL 737-1581

Fig. 5

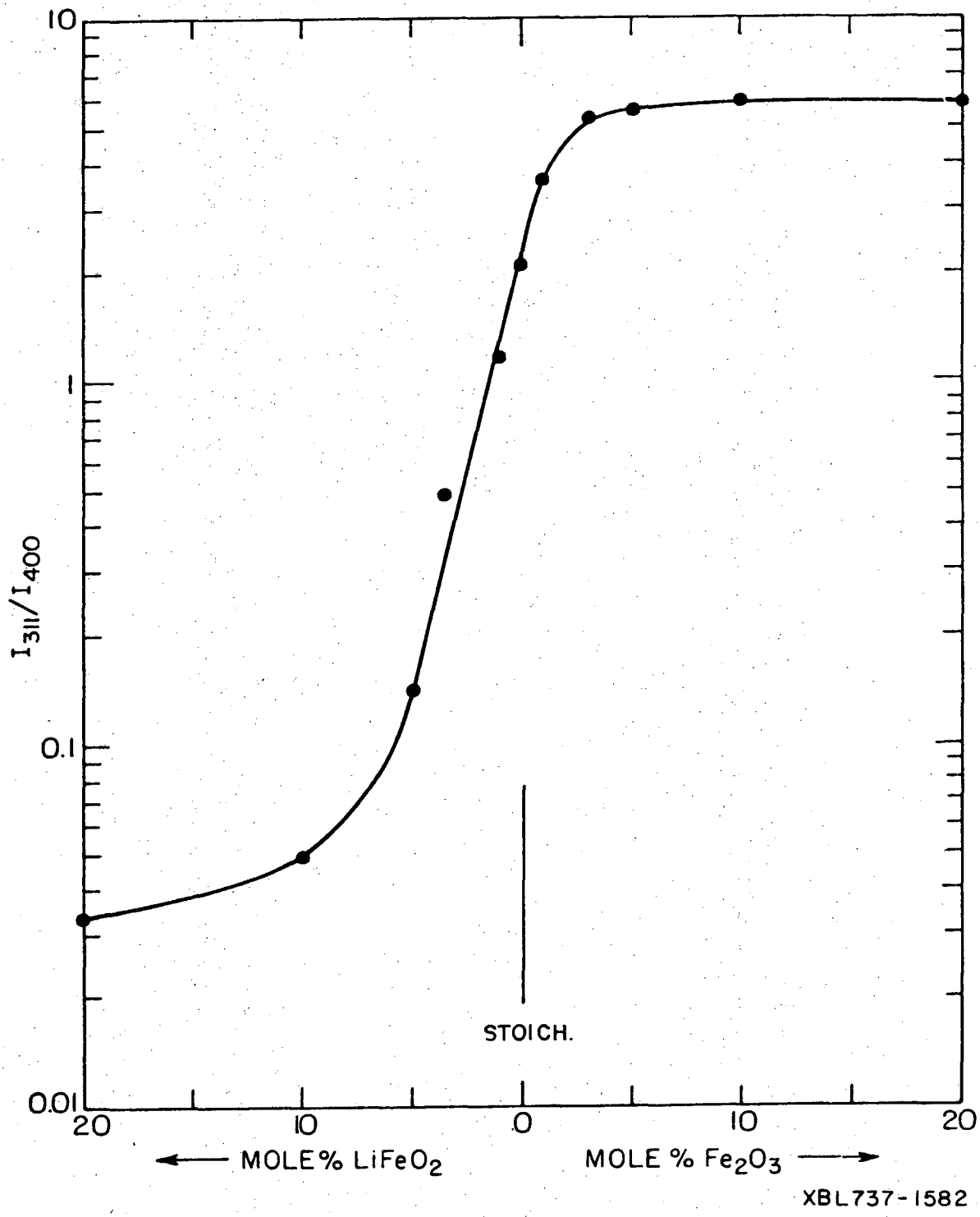
10
1
0.1
0.01
I_{311}/I_{400}
STOICH.
20
10
0
10
20
← MOLE% $LiFeO_2$
MOLE % Fe_2O_3 →
XBL737-1582

Fig. 6

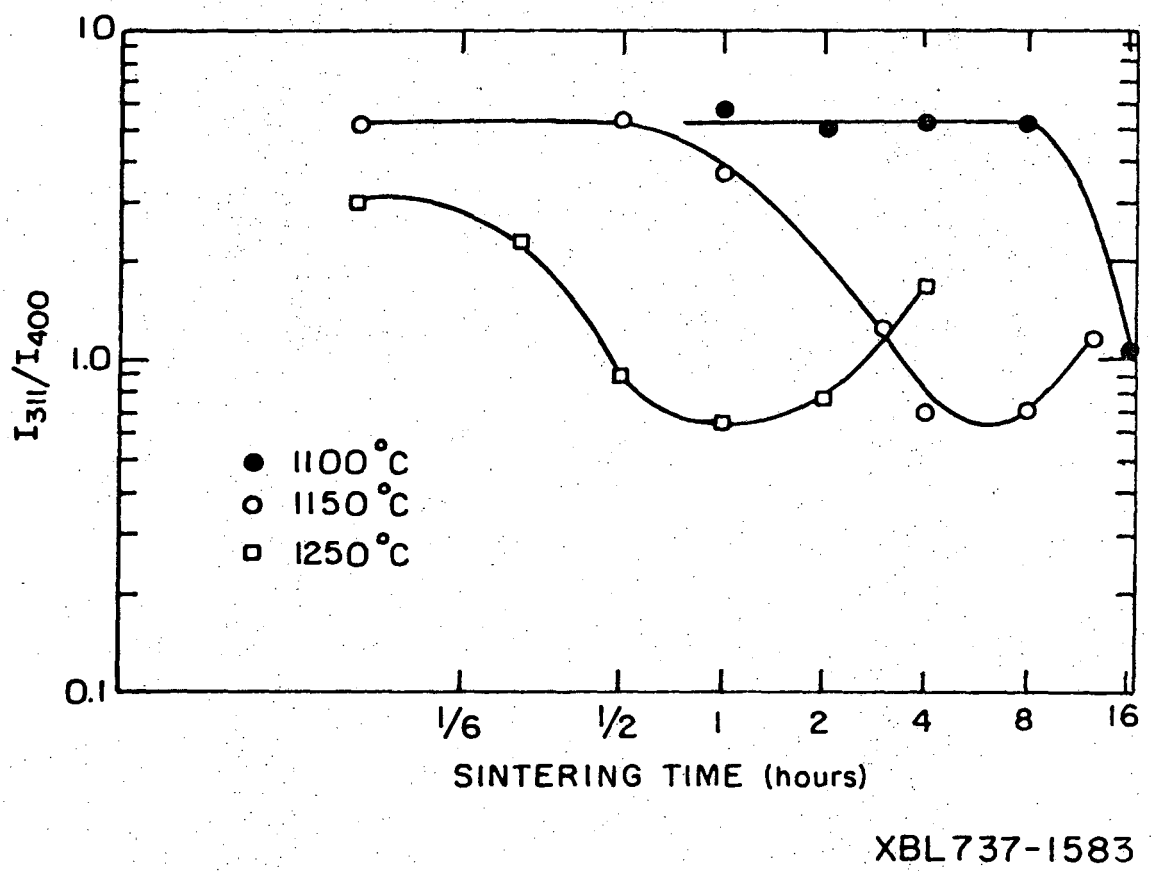
10
1.0
0.1
I_{311}/I_{400}
1100°C
1150°C
1250°C
1/6
1/2
1
2
4
8
16
SINTERING TIME (hours)
XBL737-1583

Fig. 7

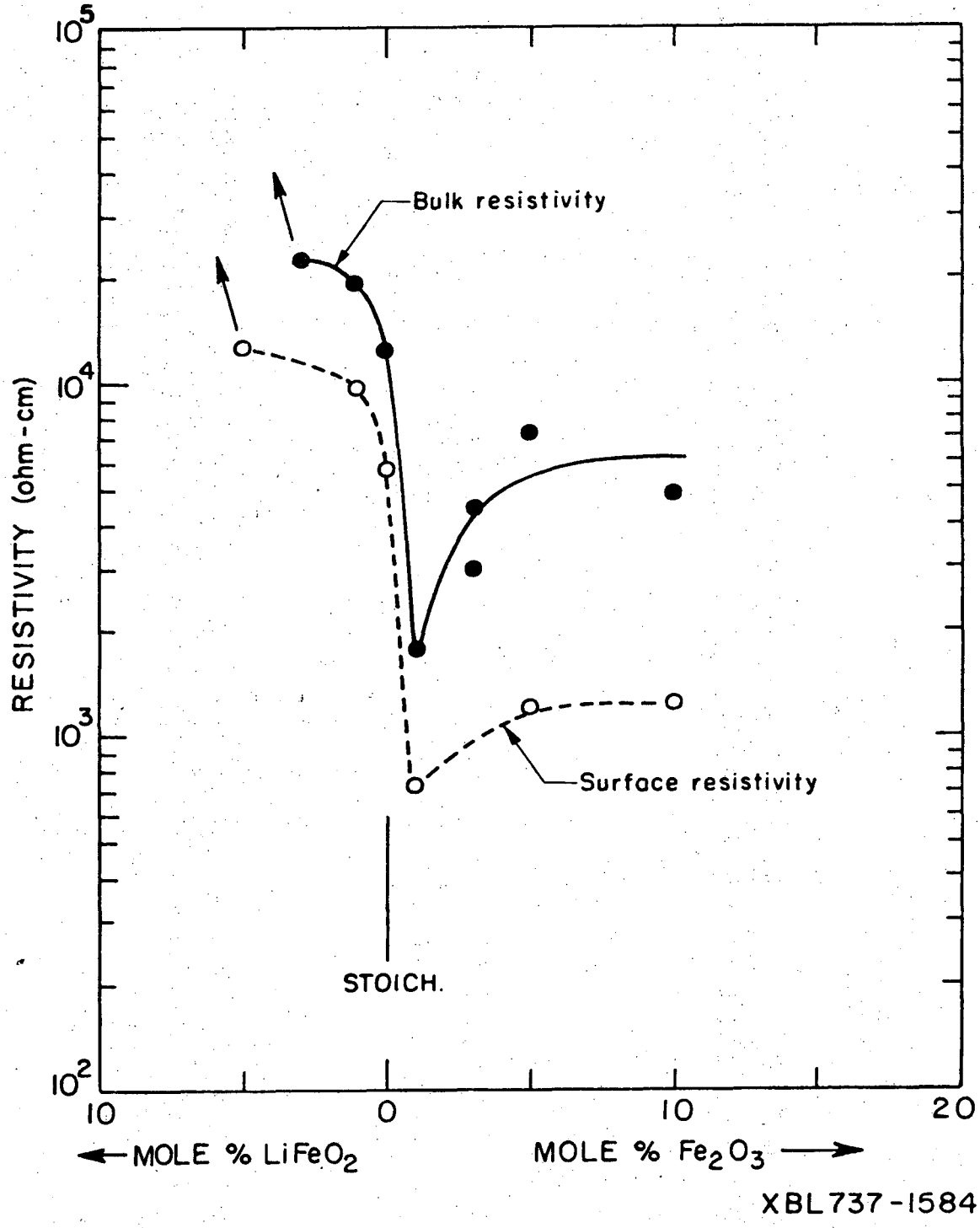
10^5
10^4
10^3
10^2
RESISTIVITY (ohm-cm)
Bulk resistivity
Surface resistivity
STOICH.
10
0
10
20
← MOLE % $LiFeO_2$
MOLE % Fe_2O_3 →
XBL737-1584

Fig. 8

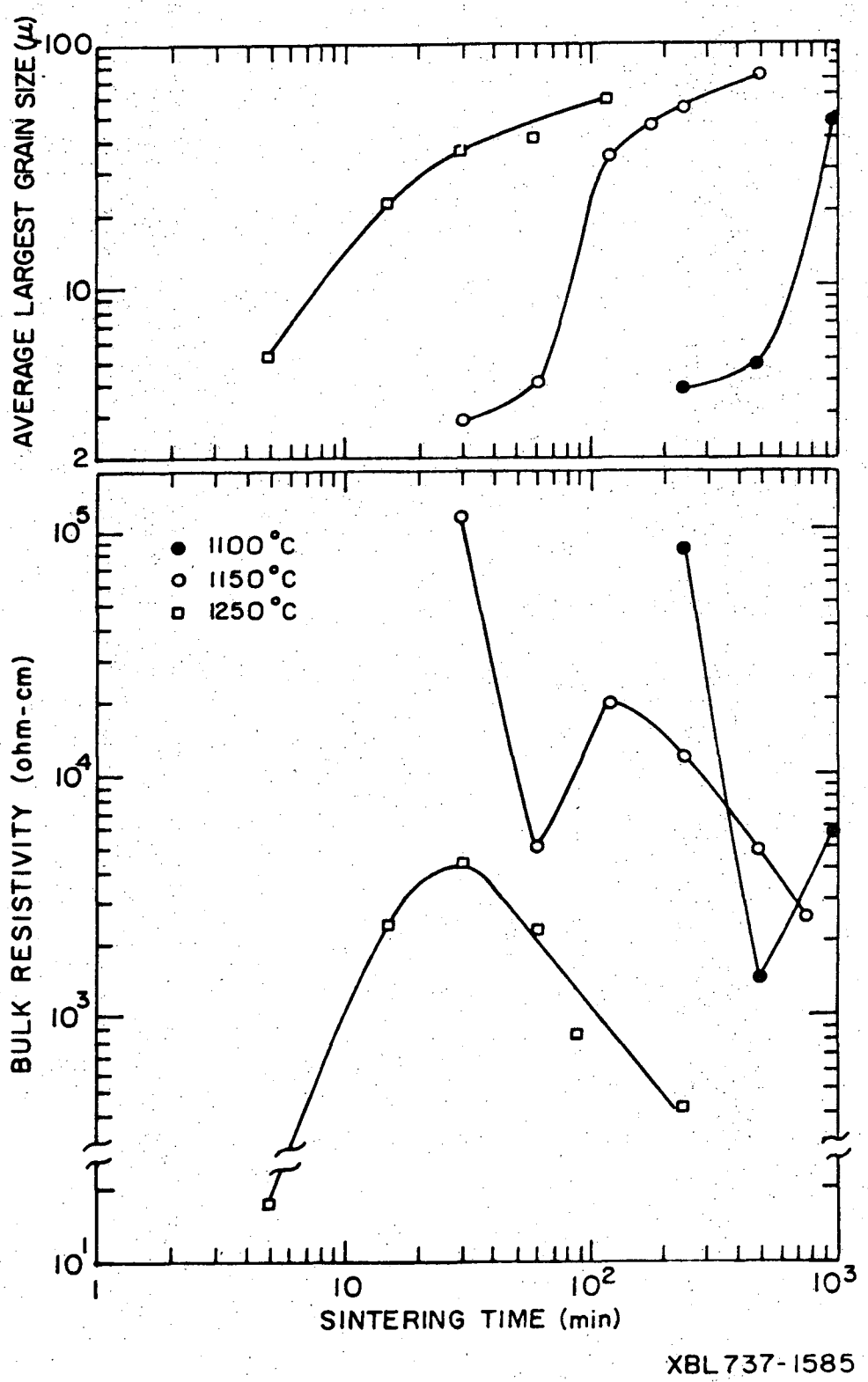
AVERAGE LARGEST GRAIN SIZE (μ)
100
10
2
BULK RESISTIVITY (ohm-cm)
10^5
10^4
10^3
10^1
1100°C
1150°C
1250°C
1
10
10^2
10^3
SINTERING TIME (min)
XBL 737-1585

Fig. 9

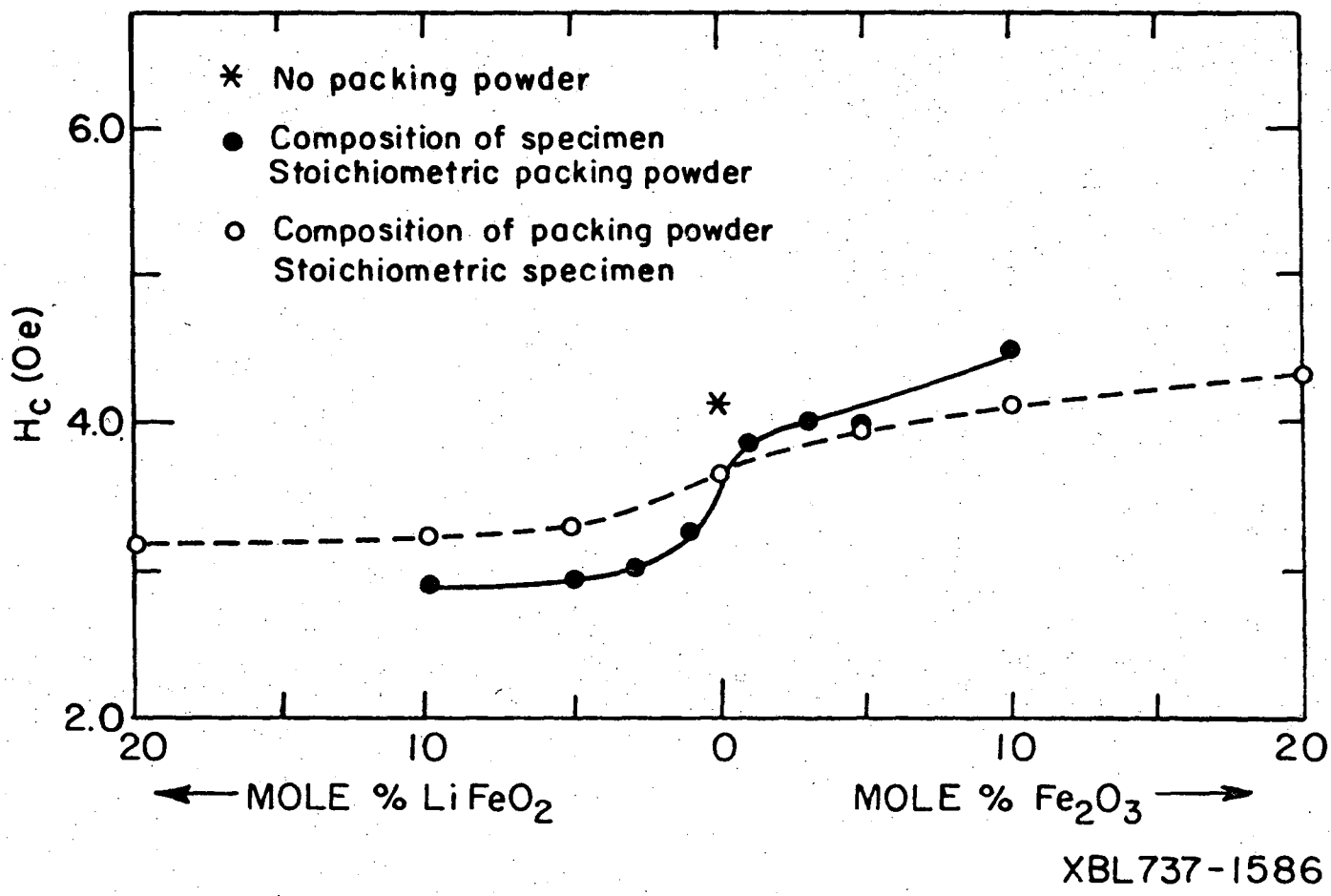
* No packing powder
● Composition of specimen
Stoichiometric packing powder
o Composition of packing powder
Stoichiometric specimen
H_c (Oe)
6.0
4.0
2.0
20
10
0
10
20
← MOLE % $LiFeO_2$
MOLE % Fe_2O_3 →
XBL737-1586

Fig. 10

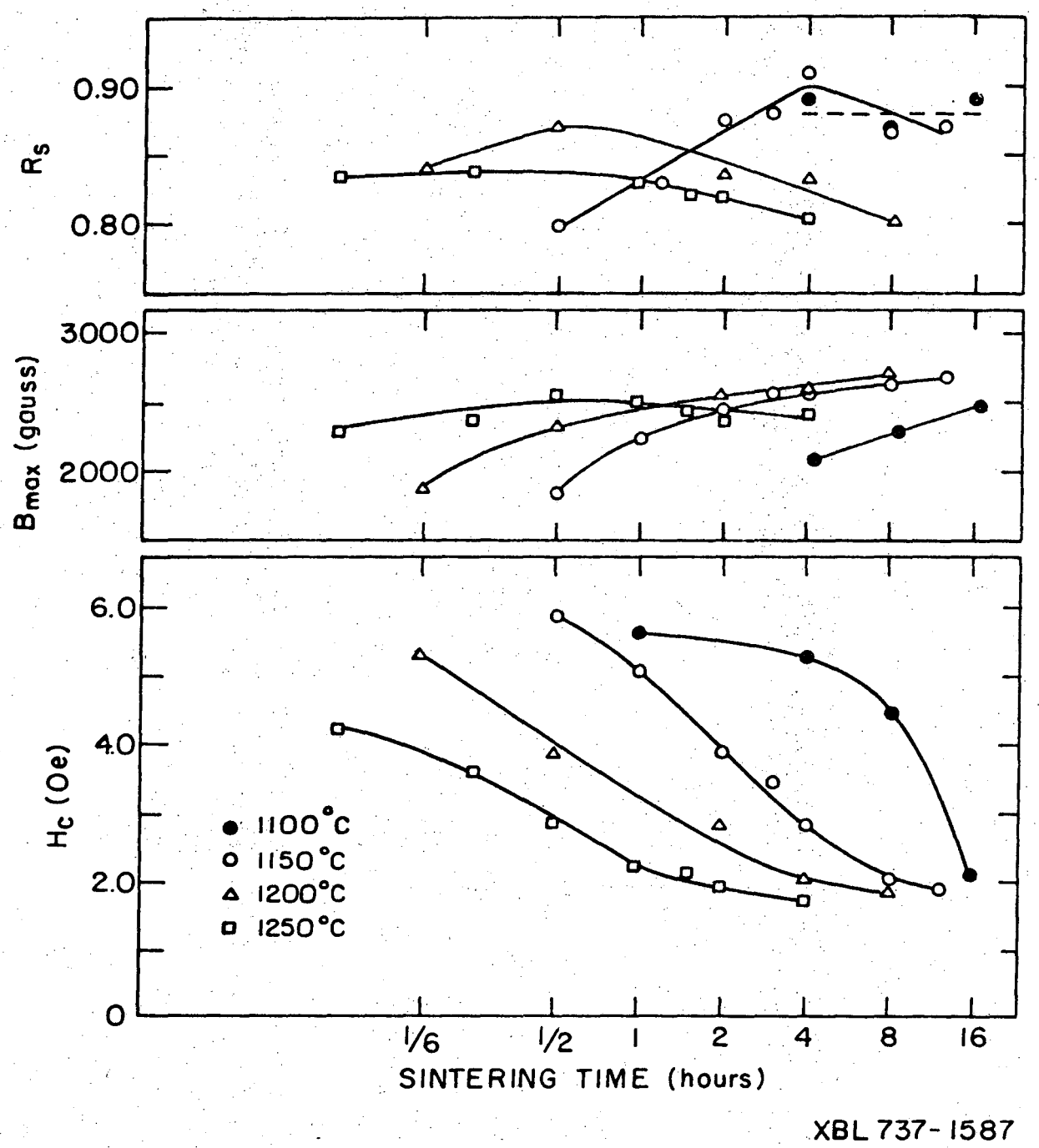
0.90
0.80
R_s
3000
2000
B_{max} (gauss)
6.0
4.0
2.0
0
H_c (Oe)
1100°C
1150°C
1200°C
1250°C
1/6
1/2
1
2
4
8
16
SINTERING TIME (hours)
XBL 737-1587

Fig. 11

TECHNICAL INFORMATION DIVISION
LAWRENCE BERKELEY LABORATORY
UNIVERSITY OF CALIFORNIA
BERKELEY, CALIFORNIA 94720